Mon. Not. R. Astron. Soc. **308**, 691–704 (1999)

The structure of superposed Weyl fields

O. Semerák,★ T. Zellerin★ and M. Žáček★
Department of Theoretical Physics, Faculty of Mathematics and Physics, Charles University, V Holešovičkách 2, CZ-180 00 Praha 8, Czech Republic

Accepted 1999 April 20. Received 1999 February 23

ABSTRACT

The properties of four superposed static axisymmetric (Weyl) space–times are illustrated by plotting their gravitational field lines and the shapes of their event horizons. The superpositions considered represent multiple Weyl systems, which are the most realistic astrophysically: the Schwarzschild black hole and the Appell ring are chosen as 'background' sources (each of them bears some features of the *non*-static Kerr source), and the Bach–Weyl ring and the 'annular' disc (inverted first Morgan–Morgan disc) of Lemos & Letelier are considered in their equatorial planes as additional sources. We study the influence of the parameters of additional sources on the fields of the central bodies.

Key words: black hole physics – gravitation – relativity.

1 INTRODUCTION

Black holes are today considered a possible, sometimes inevitable, outcome of stellar and galactic evolution. They even play a key role in the models of some astrophysical objects. In particular, a standard idea of active galactic nuclei and of some types of X-ray binaries is based on interaction of a rotating black hole with a surrounding accretion disc (e.g. Blandford 1987; Rees 1998). Regarding the usual symmetry of these systems, and also the Bardeen–Petterson effect (Bardeen & Petterson 1975), the disc is presumed to reside in the equatorial plane of the hole.

A real accretion disc is likely to have non-stationary and non-symmetric complex structure. For computational reasons, however, a 'standard model' of disc accretion has usually been employed as an approximation. Here the disc is taken to be smooth, axisymmetric and described by just a few parameters. Non-relativistic (magneto)hydrodynamics and radiative transfer are used to calculate the observable effects. The central black hole (of mass M) is treated as a Newtonian body, the gravitational field of which is described by the simple potential $-M/(r-2M)$ of Paczyński & Wiita (1980). It has been pointed out, however, that the above simplifications may lead to theories far from reality (e.g. Abramowicz 1987), and the standard model is being improved in various respects, e.g. to involve more parameters, to use general relativity (at least) in description of the central hole, and to deal with *rotating* black holes (cf. Bardeen 1970); see Kato, Fukue & Mineshige (1998) for a review.

One should also allow for self-gravitation of the accreting material, because its mass may not be completely negligible with respect to that of the hole, and because it may in fact bear most of the angular momentum of the system. The self-gravity of the disc can modify the accretion flow at the inner edge of the disc where the gas has the largest density and speed. Just there, however, it has the highest temperature and generates most of the radiation. Also the overall characteristics and stability of the disc might be sensitive to the details of a gravitational field, in particular to the mass of the disc (e.g. Abramowicz et al. 1984; Shlosman & Begelman 1987; Goodman & Narayan 1988; Chakrabarti 1988; Nishida & Eriguchi 1996, and references therein).

Switching on the self-gravity of the additional matter around the black hole is also interesting from the point of view of general relativity itself: the study of the gravitational fields of multiple systems is a natural step from isolated sources or from uniformly distributed matter. Owing to the non-linearity of Einstein equations, however, explicit results have only been reached in special cases with a high degree of symmetry. Regarding the geometry presumed in hole + disc systems, astrophysically the most relevant superposed solutions are those describing the fields of *stationary axisymmetric* sources around rotating (Kerr) black holes.

2 STATIONARY AXISYMMETRIC SOURCES AROUND BLACK HOLES

Stationary axisymmetric fields that describe rotating black holes with additional matter (usually rings, discs or tori) are found in three ways: by numerical solution of Einstein equations, by perturbations of black hole space–times and by exact analytical solutions of Einstein equations. [In the following, we do not review superpositions, obtained in either of these ways, of black holes with external *electromagnetic* fields. We refer to a review by Aliev & Gal'tsov (1989) and, for the static case, also to a paper by Alekseev & Garcia (1996).]

Numerical space–times containing a rotating black hole plus an additional stationary axisymmetric source were constructed by

★ E-mail: semerak@mbox.troja.mff.cuni.cz (OS); zellerin@falcor.karlin.mff.cuni.cz (TZ); zacek@mbox.troja.mff.cuni.cz (MŽ)

Lanza (1992) (hole + thin finite equatorial disc) and by Nishida & Eriguchi (1994) (hole + thick toroid).

A great deal of literature has been devoted to perturbations of black hole space–times, mainly after Teukolsky (1973) succeeded in separation of decoupled equations for perturbations of a Kerr black hole into the second-order ordinary differential equations for scalars constructed from the Weyl tensor (for gravitational perturbations) or from the electromagnetic field tensor (for electromagnetic perturbations). In a series of papers, Chandrasekhar (see his 1979 survey) solved these equations completely. Chrzanowski (1975) learned how, in principle, the perturbations of the metric tensor itself can be calculated from the solutions of the 'gravitational' Teukolsky equations. He employed this result to determine the perturbative distortion of the black hole horizon (Chrzanowski 1976); a similar problem, in stationary axisymmetric case, was also treated by Demianski (1976). Linet (1977) determined explicitly the stationary axisymmetric Green function of the Teukolsky equation. [Note that recently *gauge-invariant* perturbations of black holes have been discussed thoroughly by Fernandes & Lun (1996, 1997).] Up till now, however, the perturbation of the Schwarzschild metric by a (rotating) axisymmetric weakly gravitating thin equatorial ring, found by Will (1974) directly by solution of the perturbed Einstein equations, is the only perturbation of the given type that has been calculated explicitly.

In the present paper we consider several *exact* solutions of Einstein equations, describing a black hole with an additional source. Regarding the astrophysical motivation, those solutions that are relevant are mainly those that do not contain 'struts' and membranes – the supporting singularities, the presence of which indicates that a given system of sources cannot remain stationary (or static) according to the field equations. Multiple systems simply need something to compensate for the gravitational attraction between the masses of their components. For static sources, the only possibility among fundamental interactions is the electric repulsion between electric charges of the same sign; for rotating sources, magnetic interaction between magnetic dipole moments (repulsive in the antiparallel case) and gravitomagnetic interaction between spins (repulsive in the parallel case – e.g. Pfister & Schedel 1987) are also present. Analysis of the momentarily stationary and axisymmetric system of two identical sources was carried out by Dietz & Hoenselaers (1985) for the Kerr components (with mass M and specific rotational angular momentum a), and by Bičák & Hoenselaers (1985) and Manko, Martín & Ruiz (1994) for the Kerr–Newman components (with M, a and charge Q). Equilibrium was found to be possible just for extreme values of the charges ($Q = M$): rotating centres can remain in equilibrium only in a superextreme case of two naked singularities (which have $Q^2 + a^2 > M^2$: Parker, Ruffini & Wilkins 1973; Dietz & Hoenselaers 1985; Bretón & Manko 1995), both the magnetic dipole–dipole and gravitational spin–spin interactions being too weak to keep apart black holes (i.e. centres having $Q^2 + a^2 \leqslant M^2$). The configurations with extreme centres of the Reissner–Nordström type ($Q = M$) thus remain the only stationary (in fact static) equlibrium configurations containing more than one black hole (Gibbons 1980).

Accretion discs of astrophysical interest are likely to lie in the equatorial plane of the central black hole and unlikely to have a considerable charge, so neither spin–spin nor electromagnetic repulsion can support them. Hence, one instead refers to centrifugal force resulting from orbital motion of the material or to hoop stresses when interpreting the additional sources.

It turned out to be very difficult to superpose a Kerr black hole with an additional axisymmetric ring, disc or torus and no explicit exact solutions describing the systems of this kind have been known until now. This by no means implies that no solutions generalizing the solutions containing only isolated black holes have been found. In the previous two decades, a number of methods for the construction of stationary axisymmetric solutions of the (electro)vacuum Einstein equations have been developed. Two major approaches, developed by the end of the 1970s – the group-theoretic techniques and the soliton-theoretic (or inverse-scattering) techniques – have been analysed and related, notably by Cosgrove (1980, 1981, 1982), Hoenselaers & Dietz (1984), Letelier (1989) and Hoenselaers (1993); the cited works contain a thorough list of original references. The above techniques have also been discussed in more recent works in the context of new results, e.g. Alekseev's electrovacuum solitons and 'monodromy data transform', the Gutsunaev–Manko superposition method, Sibgatullin's integral equation or finite-gap solutions by Korotkin & Matveev (e.g. Quevedo 1992; Manko & Novikov 1992; Manko et al. 1994; Alekseev & Garcia 1996; Chaudhuri & Das 1997a,b). For other approaches, see e.g. Tanabe (1979), or the results of Nakamura (and similar ones by Kyriakopoulos), referred to and worked out by Tertychniy (1990) (see also Vein 1985).

The solution-generating techniques reproduce the already known space–times, but also provide wide families of new solutions characterized by arbitrarily large sets of free parameters. However, only a very restricted number of this variety of solutions possess a clear physical interpretation. Though several results probably represent a rotating black hole superposed with an 'external' gravitational field (e.g. Quevedo & Mashhoon 1991; Manko & Novikov 1992; Chaudhuri & Das 1997a,b), none of the latter appears to be generated by a ring, a disc or a torus [cf., however, the last paragraph of Section IV in Letelier & Oliveira (1987)].

In the special case of *static* axisymmetric (i.e. Weyl) metrics, the Einstein equations simplify considerably and superpositions are much easier (Section 3). In the present paper (Paper 1), the properties of four superposed Weyl space–times are illustrated by plotting their gravitational field lines and the shapes of their horizons. In the following paper (Semerák, Žáček & Zellerin 1999, Paper II in this issue) we compute, in the same fields, the trajectories of free point test particles. The superposed metrics considered in Section 3 contain no supporting singularities and represent, in our opinion, the fields of astrophysically the most realistic multiple Weyl systems.[1] The Schwarzschild black hole (Section 3.1) and the Appell ring (Section 3.2) are chosen as 'background' sources (their fields resemble, to some extent and each in different aspects, the *non*-static Kerr field), and the Bach–Weyl ring (Section 3.3) and the 'annular' disc (inverted first Morgan–Morgan disc) of Lemos & Letelier (Section 3.4) are considered in their equatorial planes as additional sources. In Section 4, the field lines are defined for a general stationary and static metric as integral curves of the four-acceleration field of the hypersurface-orthogonal congruence. The field lines are then plotted for the chosen particular cases, namely for a Schwarzschild black hole superposed with a Bach–Weyl ring and with a

[1] Recently Letelier & Oliveira (1998) studied the superpositions that, on the contrary, do contain singular structures; evaluating the compression on the singularity, they obtained the 'attraction force' between the superposed bodies.

Lemos–Letelier annular disc, and also for an Appell ring superposed with the same additional sources. In Section 5, horizons of these space–times are represented in suitable coordinates. Our main goal is to study the influence of the parameters of additional sources on the field of the central bodies.

3 SUPERPOSING WEYL FIELDS

Basic information on static axisymmetric (Weyl) space–times have been given in many places – see e.g. Synge (1960), Bičák, Lynden-Bell & Pichon (1993b) or Lemos & Letelier (1994). Weyl showed that in appropriate cylindrical coordinates (today referred to as canonical Weyl coordinates) (t, ρ, ϕ, z), the metric of any static axisymmetric space–time can be written in terms of just two functions, $\nu = \nu(\rho, z)$ and $\lambda = \lambda(\rho, z)$, in the form[2] (Weyl 1917)

$$ds^2 = -e^{2\nu}dt^2 + e^{-2\nu}\rho^2 d\phi^2 + e^{2(\lambda-\nu)}(d\rho^2 + dz^2), \tag{1}$$

provided that the energy–momentum tensor $T_{\alpha\beta}$ satisfies $T^{\rho}_{\rho} + T^{z}_{z} = 0$. Non-trivial Einstein equations yield

$$\rho^{-1}\nu_{,\rho} + \nu_{,\rho\rho} + \nu_{,zz} \equiv \nabla^2\nu = 4\pi e^{2(\lambda-\nu)}(T^{\phi}_{\phi} - T^{t}_{t}), \tag{2}$$

$$\rho^{-1}\lambda_{,\rho} - \nu^2_{,\rho} + \nu^2_{,z} = 4\pi(T_{\rho\rho} - T_{zz}), \tag{3}$$

$$\rho^{-1}\lambda_{,z} - 2\nu_{,\rho}\nu_{,z} = 8\pi T_{\rho z}, \tag{4}$$

$$\lambda_{,\rho\rho} + \lambda_{,zz} - \nabla^2\nu + \nu^2_{,\rho} + \nu^2_{,z} = 4\pi e^{2(\lambda-\nu)}(T^{t}_{t} + T^{\phi}_{\phi}), \tag{5}$$

where commas denote partial derivatives.

In the vacuum case ($T_{\alpha\beta} = 0$), equation (2) for ν becomes a Laplace equation,

$$\nabla^2\nu = 0, \tag{6}$$

and equations (3) and (4) for λ imply

$$\lambda = \int_{\text{axis}}^{\rho,z} \rho[(\nu^2_{,\rho} - \nu^2_{,z})\,d\rho + 2\nu_{,\rho}\nu_{,z}\,dz], \tag{7}$$

where the integration is taken along a path going from the axis ($\rho = 0$) to a given point through the region devoid of matter (note that 'elementary flatness' requires $\lambda = 0$ at the vacuum parts of the axis; see Synge 1960). Linearity of the Laplace equation for ν allows us to generate relativistic solutions from classical ones and to obtain the fields of multiple sources by linear superposition. The superposition of two vacuum Weyl fields, (ν_1, λ_1) and (ν_2, λ_2), is described by

$$\nu = \nu_1 + \nu_2 \tag{8}$$

and

$$\lambda = \lambda_1 + \lambda_2 + 2\int_{\text{axis}}^{\rho,z} \rho[(\nu_{1,\rho}\nu_{2,\rho} - \nu_{1,z}\nu_{2,z})\,d\rho + (\nu_{1,\rho}\nu_{2,z} + \nu_{1,z}\nu_{2,\rho})\,dz]. \tag{9}$$

The construction of any Weyl space–time starts from solution of the Laplace equation for the metric function ν. The Green function $G(\boldsymbol{x}, \boldsymbol{x}_0) = -(4\pi)^{-1}|\boldsymbol{x} - \boldsymbol{x}_0|^{-1}$ is often employed to find the solution by convolution with the source spatial density $w(\boldsymbol{x})$,

$$\nu(\boldsymbol{x}) = 4\pi\int_{\text{source}} w(\boldsymbol{x}')G(\boldsymbol{x}, \boldsymbol{x}')\,d^3\boldsymbol{x}'. \tag{10}$$

Another way is to transform oneself to some coordinates in which the Laplace equation separates into ordinary differential equations. Cylindrical (Weyl) and prolate spheroidal coordinates are mostly used if the source is a rod on the axis, while toroidal coordinates are suitable for ring solutions and oblate spheroidal ones for discs. We will see it in the following where particular space–times are listed which superpositions will be considered below. In these superpositions, the mass of the 'background' source will always be denoted by M, and that of the additional source by $\mathcal{M}$. The Weyl radius of the Appell ring will be a, while that of the external sources (of the Bach–Weyl ring and of the inner edge of the Lemos–Letelier annular disc) will be denoted by b.

3.1 Schwarzschild black hole

The simplest type of Weyl solution is generated by line sources lying on the axis (Levi-Civita 1919). For a homogeneous rod of mass M and length $2l$ placed about the origin ($\rho = 0$, $|z| < l$), the metric functions read, respectively in Weyl and prolate coordinates,

$$\nu = \frac{M}{2l}\ln\frac{d_1 + d_2 - 2l}{d_1 + d_2 + 2l} \tag{11}$$

$$= \frac{M}{2l}\ln\left(1 - \frac{2l}{r}\right), \tag{12}$$

$$\lambda = \frac{M^2}{2l^2}\ln\frac{(d_1 + d_2)^2 - 4l^2}{4\Sigma} \tag{13}$$

$$= \frac{M^2}{2l^2}\ln\frac{r(r - 2l)}{\Sigma}, \tag{14}$$

where

$$d_{1,2} = \sqrt{\rho^2 + (z \mp l)^2} = r - l \mp l\cos\theta \tag{15}$$

are distances from the ends of the rod, r and θ are prolate spheroidal radial and latitudinal coordinates, related to ρ and z by

$$\rho = \sqrt{r(r - 2l)}\sin\theta, \qquad z = (r - l)\cos\theta, \tag{16}$$

or

$$r - l = (d_2 + d_1)/2, \qquad l\cos\theta = (d_2 - d_1)/2, \tag{17}$$

and

$$\Sigma = d_1 d_2 = [(\rho^2 + z^2 + l^2)^2 - 4z^2l^2]^{1/2} = (r - l)^2 - l^2\cos^2\theta \tag{18}$$

stands for a square of the mean distance from the singular rod. In particular, for a single particle placed at the origin, i.e. in the limit $l \to 0$, one has the Curzon solution

$$\nu = -M/\sqrt{\rho^2 + z^2} \tag{19}$$

$$= -M/r, \tag{20}$$

$$\lambda = -\frac{1}{2}\left(\frac{M\rho}{\rho^2 + z^2}\right)^2 \tag{21}$$

$$= -\frac{1}{2}\left(\frac{M\sin\theta}{r}\right)^2. \tag{22}$$

[2] The signature of the metric will be $-+++$; Greek indices run from 0–3 and Latin indices from 1–3. We use geometrized units in which $c = G = 1$, c being the speed of light in a vacuum and G the gravitational constant.

Another special case is the Schwarzschild solution that is obtained with $l = M$ (then r and θ are Schwarzschild coordinates).

3.2 Appell ring

In last-century electrodynamics, an interesting solution (by Appell) of the Laplace equation appeared, generated by a particle with charge (here mass) M situated on imaginary extension of the axis – at $\rho = 0$ and $z = \mathrm{i}a$, a being some positive real distance; see the first member of the ring family of solutions of Letelier & Oliveira (1987) and Gleiser & Pullin (1989) with their $\alpha = 0$. The real part of the corresponding complex potential $-M/[\sqrt{\rho^2 + (z - \mathrm{i}a)^2}]$ gives a real solution

$$\nu = -\frac{M}{\sqrt{2\Sigma}}(\Sigma + \rho^2 + z^2 - a^2)^{1/2} \tag{23}$$

$$= -\frac{M}{\sqrt{\Sigma}}\cos(\psi/2) \tag{24}$$

$$= -Mr/\Sigma, \tag{25}$$

where r and θ are now oblate spheroidal coordinates,[3] given by

$$\rho = \sqrt{r^2 + a^2}\sin\theta, \qquad z = r\cos\theta, \tag{26}$$

or

$$\sqrt{r^2 + a^2} = (d_2 + d_1)/2, \qquad a\sin\theta = (d_2 - d_1)/2, \tag{27}$$

and we have used also toroidal coordinates ζ and ψ, related to ρ and z by

$$\rho = (\Sigma/2a)\sinh\zeta, \qquad z = (\Sigma/2a)\sin\psi, \tag{28}$$

[the inverse transformation is obtained trivially by using $\Sigma(\zeta,\psi)$ from below]. Again,

$$d_{1,2} = \sqrt{(\rho \mp a)^2 + z^2} = \sqrt{r^2 + a^2} \mp a\sin\theta \tag{29}$$

denote extreme distances and

$$\Sigma = d_1 d_2 = [(\rho^2 + z^2 + a^2)^2 - 4\rho^2 a^2]^{1/2}$$

$$= 2a^2/(\cosh\zeta - \cos\psi) = r^2 + a^2\cos^2\theta \tag{30}$$

is the square of the mean distance from the source (i.e. from the singular ring at $\rho = a$, $z = 0$) within the (ρ, z) plane.

The second metric function reads, respectively in the Weyl, toroidal and oblate spheroidal coordinates,

$$\lambda = \frac{M^2}{8a^2}\left[1 - \frac{\rho^2 + z^2 + a^2}{\Sigma} - \frac{2a^2\rho^2(\Sigma^2 - 8z^2a^2)}{\Sigma^4}\right] \tag{31}$$

$$= \frac{M^2}{16a^2}(2 - 2\cosh\zeta - \sinh^2\zeta\cos 2\psi) \tag{32}$$

$$= -\frac{M^2\sin^2\theta}{4\Sigma}\left[1 + \frac{(r^2 + a^2)(\Sigma^2 - 8r^2a^2\cos^2\theta)}{\Sigma^3}\right] \tag{33}$$

[this is 1/16 of the expression given by Gleiser & Pullin (1989)].

[3] We use the same letters as for prolate spheroidal coordinates defined in previous section (which yield Schwarzschild coordinates for $l = M$). This should not cause confusion – only in Section 5 will we transform explicitly from prolate to Schwarzschild coordinates.

In the limit $a \to 0$, the Curzon solution (19)–(22) is obtained again.

Global structure of the Appell space–time is the same as that of the Kerr space–time, and also the local properties of the fields are somewhat similar. The main features of the Kerr solution are the occurrence of the horizon (if $a \leqslant M$) and of the rotational dragging that gives rise to the ergosphere. These features, however, cannot be expected to be present in the Appell solution (or in *any* static solution treated in Weyl coordinates). The resemblance of the Appell and Kerr fields is discussed in the Appendix. In the context of *stationary* situations, the Schwarzschild and Appell fields can be considered as different static approximations involving some of the properties of a *rotating* black hole.

3.3 Bach–Weyl ring

The field of a 'normal' ring (placed at $z = 0$, $\rho = b$) is different from the Appell one. Its global structure in Weyl coordinates is simpler (it is not double-sheeted), although the ring itself also has non-trivial structure – it again forms a directional singularity (Hoenselaers 1995), known from rotating line sources as the Kerr ring (Hoenselaers 1990; Punsly 1990). The respective metric functions are more complicated, namely given by elliptic integrals (Bach & Weyl 1922):

$$\nu = -\frac{2\mathcal{M}K(k)}{\pi d_2}, \tag{34}$$

$$\lambda = \frac{\mathcal{M}^2k^4}{4\pi^2b^2\rho}[(\rho + b)(-K^2 + 4k'^2K\dot{K} + 4k^2k'^2\dot{K}^2)$$

$$- 4\rho k^2k'^2(k'^2 + 2)\dot{K}^2], \tag{35}$$

where $\mathcal{M}$ is mass of the ring, $K(k)$ is the complete Legendre elliptic integral of the first kind, $\dot{K} = \mathrm{d}K/\mathrm{d}(k^2)$, $k'^2 = d_1^2/d_2^2$, $k^2 = 1 - k'^2 = 4b\rho/d_2^2$ and $d_{1,2} = \sqrt{(\rho \mp b)^2 + z^2}$, similarly to the previous section.

The potential ν can also be written as a series of Legendre polynomials,

$$\nu = -\mathcal{M}\sum_{n=0}^{\infty}\frac{(\rho^2 + z^2)^n}{b^{2n+1}}P_{2n}\left(\frac{z}{\sqrt{\rho^2 + z^2}}\right)P_{2n}(0) \tag{36}$$

for $\rho^2 + z^2 < b^2$ and

$$\nu = -\mathcal{M}\sum_{n=0}^{\infty}\frac{b^{2n}}{(\rho^2 + z^2)^{n+1/2}}P_{2n}\left(\frac{z}{\sqrt{\rho^2 + z^2}}\right)P_{2n}(0) \tag{37}$$

for $\rho^2 + z^2 > b^2$. Each of the above terms is itself a solution of the Laplace equation, so one can cut the sum anywhere and always obtains a field of *some* matter distribution. However, this may differ from that of a ring considerably because of the rather bad convergence of the above series, mainly at $\rho^2 + z^2 \sim b^2$ (cf. Fig. 1). For numerical solutions, it is better to use the form (34), where the elliptic integral can be computed very effectively in terms of series by the method of arithmetic–geometric mean (a sum of five terms is accurate to some 28 digits here).

3.4 Inverted first Morgan–Morgan disc

The simplest two-dimensional Weyl source is an (uncharged)

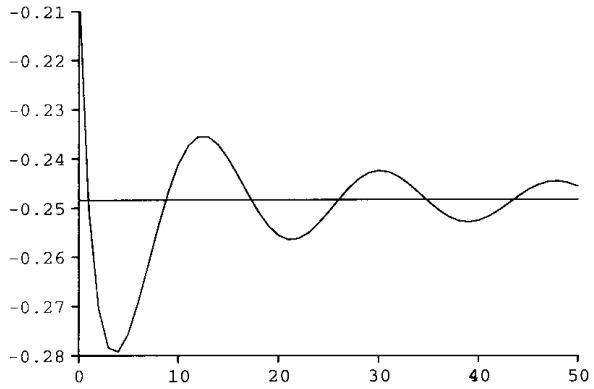

Figure 1. The dependence on the number of terms n of the sum (36,37) for a Bach–Weyl ring of mass $\mathcal{M}$ and Schwarzschild-type radius $r = 6\mathcal{M}$, calculated at $r = 5.997\mathcal{M}$, $\theta = 80°$ (there $\rho^2 + z^2 = b^2$, which is the case of worst convergence). One finds that at $n = 50$ the sum still oscillates by several per cent about the final result $\nu \doteq -0.2484$. Hence, it is rather risky to add e.g. just $n \leqslant 3$ terms like Chakrabarti (1988), and even the extension to $n = 50$ (Khanna & Chakrabarti 1992, section 3) may occasionally turn out to be problematic, mainly in calculations involving derivatives.

axisymmetric thin equatorial disc. In order to remain static, it must be supported by hoop stresses or by inertia of two equal streams of dust which circulate in opposite directions around the centre of the disc. The metric for a general static thin counter-rotating disc was given by Bičák, Lynden-Bell & Katz (1993a), who also showed that most vacuum Weyl fields are its special cases. For a finite disc, the solution for ν (given as a series in products of the Legendre polynomials and Legendre functions of the second kind) is singular on the rim of the disc in general. The simplest singularity-free case was found by Morgan & Morgan (1969). Its Newtonian source density is

$$w(\rho, z) = \frac{3\mathcal{M}}{2\pi b^3}\sqrt{b^2 - \rho^2}\,\delta(z) \tag{38}$$

and the metric potentials are

$$\nu = -(3\mathcal{M}/4b)[(3\cos^2\theta - 1)(r/b)A + (1 + \cos^2\theta)\mathrm{arccot}(r/b)], \tag{39}$$

$$\lambda = (3\mathcal{M}\rho/2b^2)^2[(\rho B/b)^2 - (1 + \cos^2\theta)A^2 - 2(r/b)AB\sin^2\theta], \tag{40}$$

where $A = (r/b)\mathrm{arccot}(r/b) - 1$, $B = (1/2)[r/(r + b) - \mathrm{arccot}(r/b)]$, and r and θ are oblate spheroidal coordinates defined as in Section 3.2.

Note here that the whole family of Weyl discs and rings was considered by Letelier & Oliveira (1987) as seed solutions for generation of *stationary* disc and ring space–times. The Morgan–Morgan disc is the first ($n = 1$) member of the disc family, given by Newtonian densities $w_n = [(2n + 1)\mathcal{M}/(2\pi b^3)] \times (b^2 - \rho^2)^{n-1/2}\delta(z)$. The zeroth member of the associated ring family is the Appell solution.

The Morgan–Morgan discs have an outer edge (at $\rho = b$) but not an inner one, which makes their superposition with a central body problematic. In particular, in superposition of these discs with a black hole, regions develop where the counter-rotating streams would have to move with tachyonic speeds (in order to stay on the orbit), because the disc matter reaches up to the horizon (at $\rho = 0$). Lemos & Letelier (1994) proposed to

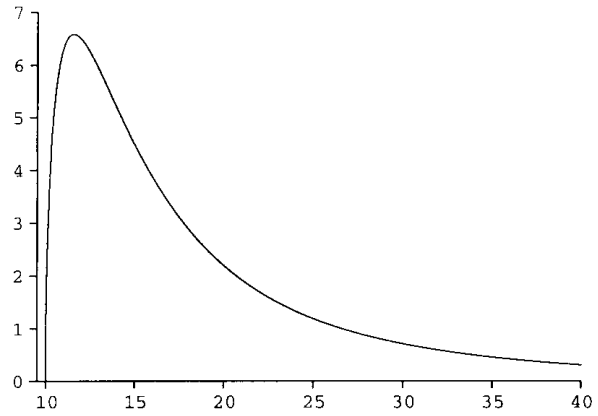

Figure 2. Surface density profile (42) of the inverted Morgan–Morgan disc. The maximum reaches $(3\sqrt{3}\mathcal{M})/(8\pi^2 b^2)$ and lies very close to the edge of the disc – at $\rho = (2/\sqrt{3})b \doteq 1.115b$. The density of the actual accretion disc is supposed to be of similar shape. In the plot we choose $b = 10\mathcal{M}$; the ρ-axis (horizontal) is in units of $\mathcal{M}$, the vertical one is in units of $\mathcal{M}^{-1}$.

overcome this by making an inversion (Kelvin transformation)

$$\rho \to \frac{b^2\rho}{\rho^2 + z^2}, \qquad z \to \frac{b^2 z}{\rho^2 + z^2} \tag{41}$$

of the Morgan–Morgan solution, which yields a disc with an *inner* rim (at $\rho = b$), namely with the density

$$w(\rho, z) = \frac{2\mathcal{M}b}{\pi^2\rho^4}\sqrt{\rho^2 - b^2}\,\delta(z) \tag{42}$$

(its profile is shown in Fig. 2). They found that the potential of the inverted disc is related to the original one according to

$$\nu(\rho, z) \to \frac{4b}{3\pi\sqrt{\rho^2 + z^2}}\,\nu\left(\frac{b^2\rho}{\rho^2 + z^2}, \frac{b^2 z}{\rho^2 + z^2}\right). \tag{43}$$

[The expression given in Lemos & Letelier (1994) must be multiplied by $4/3\pi$ in order to vary exactly as $\nu \sim -\mathcal{M}/\sqrt{\rho^2 + z^2}$ far from the source. Also, their inverted Morgan–Morgan density must be multiplied by the same factor in order to read as (42) and to really yield $\int\int\int w(\rho, z)\rho\,\mathrm{d}\rho\,\mathrm{d}\phi\,\mathrm{d}z = \mathcal{M}$.] This means

$$\nu\left(\frac{r^2}{b^2}, \cos^2\theta\right) \to \frac{4b}{3\pi\sqrt{r^2 + b^2\sin^2\theta}}\,\nu\left(\frac{b^2\cos^2\theta}{r^2 + b^2\sin^2\theta}, \frac{r^2}{r^2 + b^2\sin^2\theta}\right) \tag{44}$$

in terms of oblate coordinates, so the solution (39) transforms into

$$\nu = -\frac{\mathcal{M}}{\pi(r^2 + b^2\sin^2\theta)^{3/2}} \times \left[(2r^2 - b^2\sin^2\theta)\frac{b|\cos\theta|}{\sqrt{r^2 + b^2\sin^2\theta}}A + (2r^2 + b^2\sin^2\theta)\,\mathrm{arccot}\left(\frac{b|\cos\theta|}{\sqrt{r^2 + b^2\sin^2\theta}}\right)\right], \tag{45}$$

where

$$A = \frac{b|\cos\theta|}{\sqrt{r^2 + b^2\sin^2\theta}}\,\mathrm{arccot}\left(\frac{b|\cos\theta|}{\sqrt{r^2 + b^2\sin^2\theta}}\right) - 1.$$

As already stated by Lemos & Letelier (1994), it is not trivial to find the other metric function λ by analytical methods; instead we will compute it numerically when needed.

It was shown in Lemos & Letelier (1994) that the inverted first Morgan–Morgan family of annular discs allows one to construct realistic configurations mimicking a true accretion disc around a static black hole. In particular, the disc can be chosen free of non-physical regions (with negative pressure or/and superluminal speed of particles) and with its inner edge lying somewhere at the last stable circular geodesic about the central hole.

4 GRAVITATIONAL FIELD LINES IN SUPERPOSED SPACE–TIMES

Let us consider a *stationary* axisymmetric space–time and write down its metric in cylindrical-type (Weyl–Lewis–Papapetrou) coordinates (t, ρ, ϕ, z) attached to the symmetries

$$\mathrm{d}s^2 = g_{tt}\,\mathrm{d}t^2 + 2g_{t\phi}\,\mathrm{d}t\,\mathrm{d}\phi + g_{\phi\phi}\,\mathrm{d}\phi^2 + g_{\rho\rho}\,\mathrm{d}\rho^2 + g_{zz}\,\mathrm{d}z^2, \qquad (46)$$

where $g_{\alpha\beta}$ depend only on ρ and z and the metric functions g_{tt}, $g_{t\phi}$, $g_{\phi\phi}$ are given invariantly in terms of the two existing Killing vector fields $\eta^\alpha = \partial x^\alpha/\partial t$ and $\xi^\alpha = \partial x^\alpha/\partial\phi$:

$$g_{tt} = \eta_\iota\eta^\iota, \qquad g_{t\phi} = \eta_\iota\xi^\iota, \qquad g_{\phi\phi} = \xi_\iota\xi^\iota. \qquad (47)$$

In a stationary axisymmetric field, the simplest type of world lines are spatially circular orbits, given by $\rho =$ constant, $z =$ constant and $\Omega = \mathrm{d}\phi/\mathrm{d}t =$ constant. They follow the background symmetries (the tangent to each of these orbits is a Killing vector), hence all of their characteristics are independent of t and ϕ (thus also of the proper time τ). In particular, the observers who move along them see an unchanging field in their nearby surroundings, thus being called stationary and used frequently as reference observers in 1 + 3 splittings and interpretations. Their four-velocity is

$$u^\alpha = u^t(1, 0, \Omega, 0),$$
$$u^t = (-g_{tt} - 2g_{t\phi}\Omega - g_{\phi\phi}\Omega^2)^{-1/2}, \qquad (48)$$

and their four-acceleration is

$$a_\alpha = -\frac{1}{2}g_{\iota\kappa,\alpha}u^\iota u^\kappa \qquad (49)$$

(it has only ρ and z components).

Incited by certain counterintuitive relativistic effects in strong fields around black holes, a considerable interest has recently been devoted to an interpretation of relativistic motion in terms of 'forces', defined in analogy with classical physics. Though there is no physically unique way to define individual 'forces' in relativity, and several different approaches have been proposed, there is an agreement (modulo the boost factor, if any) in what to call the 'gravitoelectric' or 'gravitational' (perhaps also 'scalar', 'Newtonian', 'Schwarzschild' or 'static') component of the source field (e.g. Greene, Schucking & Vishveshwara 1975; Thorne, Price & Macdonald 1986; Jantzen, Carini & Bini 1992; Abramowicz, Nurowski & Wex 1993; Semerák 1995; Barrabès, Boisseau & Israel 1995): it is generated by mass density and given by the four-acceleration field of the hypersurface-orthogonal congruence. In stationary axisymmetric space–times the latter is represented by a particular case of stationary observers with zero angular momentum with respect to the axis of symmetry (ZAMOs). Their azimuthal angular velocity

$$\Omega = \Omega_{\mathrm{ZAMO}} = -g_{t\phi}/g_{\phi\phi} \equiv \omega \qquad (50)$$

is interpreted as the angular velocity of the space–time geometry, dragged into corotation with the source. The four-velocity u^α then has the time component

$$u^t = (-g_{tt} - g_{t\phi}\omega)^{-1/2} = \sqrt{-g^{tt}}. \qquad (51)$$

In *static* axisymmetric (Weyl) space–times, $g_{t\phi} = 0$ (there is no 'gravitomagnetic' component of the field, no dragging), so $\omega = 0$ and ZAMOs become static observers having

$$u^t = (-g_{tt})^{-1/2} \qquad (52)$$

and

$$a_\alpha = \frac{g_{tt,\alpha}}{2g_{tt}} = \frac{1}{2}[\ln(-g_{tt})]_{,\alpha}. \qquad (53)$$

Writing $g_{tt} = -\mathrm{e}^{2\nu}$ as in previous sections, this is simply

$$a_\alpha = \nu_{,\alpha}. \qquad (54)$$

Therefore, to draw the gravitational field lines of Weyl space–times, it is sufficient to know the potential ν; the other metric function λ is not required.

For the Schwarzschild field, a_α has only a radial component (in Schwarzschild coordinates),

$$a_r = \frac{M}{r(r-2M)}, \qquad (55)$$

while for the Appell field, in oblate coordinates,

$$(a_r, a_\theta) = (M/\Sigma^2)(r^2 - a^2\cos^2\theta, -ra^2\sin 2\theta). \qquad (56)$$

The fields of the additional sources are somewhat more complicated. In oblate coordinates, one has

$$(a_r, a_\theta) = \frac{2\mathcal{M}}{\pi d_2^4}\left[\frac{r}{\sqrt{r^2+b^2}}(d_2^2K + 4d_1\dot{K}b\sin\theta),\right.$$
$$\left. b\cos\theta(d_2^2K - 4d_1\dot{K}\sqrt{r^2+b^2})\right] \qquad (57)$$

for the Bach–Weyl ring, while for the Lemos–Letelier annular disc

$$a_r = \frac{\mathcal{M}r}{\pi(r^2+b^2\sin^2\theta)^3}$$
$$\times\left\{\left[3(2r^2-3b^2\sin^2\theta)A - 2\frac{r^2+b^2\sin^2\theta}{r^2+b^2}b^2\sin^2\theta\right]\right.$$
$$\times b|\cos\theta| + (2r^2 - b^2\sin^2\theta)\sqrt{r^2+b^2\sin^2\theta}$$
$$\left.\times\mathrm{arccot}\left(\frac{b|\cos\theta|}{\sqrt{r^2+b^2\sin^2\theta}}\right)\right\}, \qquad (58)$$

$$a_\theta = \frac{\mathcal{M}b|\cos\theta|\tan\theta}{\pi(r^2+b^2\sin^2\theta)^3}\{[(8r^2 - b^2\sin^2\theta)(r^2+b^2) + 2(2r^2$$
$$- b^2\sin^2\theta)b^2\cos^2\theta]A + (4r^2 - b^2\sin^2\theta)(r^2 + b^2\sin^2\theta)\}, \qquad (59)$$

where A is defined as in equation (45).

In Figs 3–6 we deal with four types of superpositions – of the Schwarzschild black hole or the Appell ring of radius $\rho = a(= 3M)$ with the equatorial Bach–Weyl ring or the Lemos–Letelier

annular disc. Three different masses of the external sources are chosen, $\mathcal{M} = 0.1M$, M and $10M$, M being mass of the central source; the unrealistic, 'supermassive' case of $\mathcal{M} = 10M$ is included just for interest, as it demonstrates what a strong source the black hole is. The 'external' sources (namely the ring and the inner edge of the disc) are placed near the last stable circular equatorial geodesic of the 'background' space–time, which lies at $r = 6M$ in the Schwarzschild case and at $\rho \doteq 9.6M$ in the Appell case (see Paper II for further discussion on this point). The plots are to be compared with the structure of the pure backgrounds; the Schwarzschild field lines are known to be purely radial, and those of the Appell space–time considered here are given in the Appendix.

The field lines are followed within the interesting, strong-field central regions of the superposed space–times, in meridional sections of natural coordinates of the background source, i.e. of (prolate) Schwarzschild coordinates for the Schwarzschild centre, or in Weyl axes with the mesh of oblate coordinates for the Appell centre. The field lines appear as solid lines in each of the plots, as well as the axes (which are $r\sin\theta$, $r\cos\theta$ in the case of a

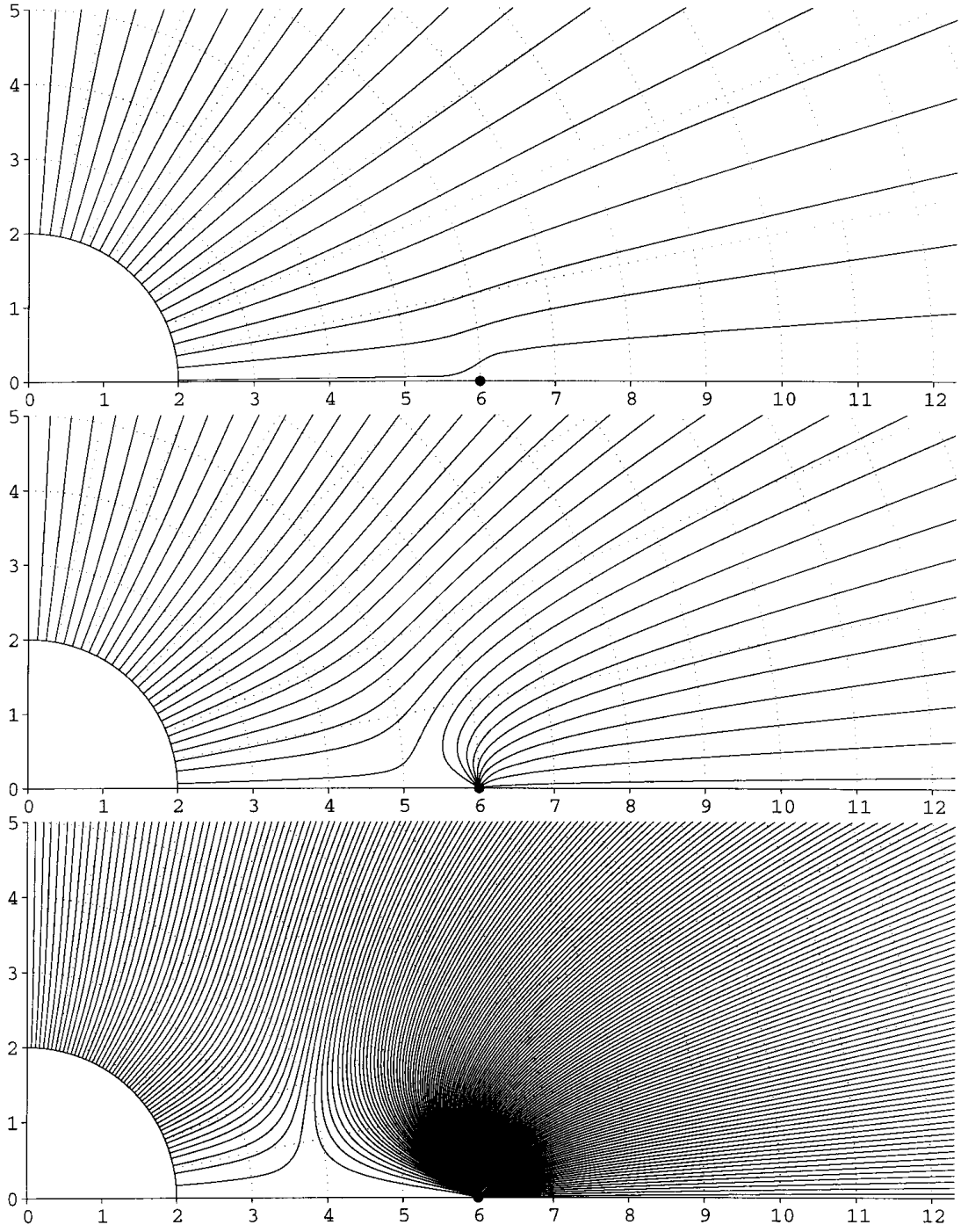

Figure 3. Field lines in the space–times of a Schwarzschild black hole (of mass M) with a Bach–Weyl ring, drawn in Schwarzschild coordinates. The ring is placed at $\theta = 90°$, $r = 6M$ and has mass $\mathcal{M} = 0.1M$, M and $10M$ as taken from top to bottom.

Schwarzschild centre, and ρ, z in the case of an Appell centre). The empty quarter-circle at $r = 2M$ (in Figs 3 and 4) is a Schwarzschild horizon; the solid abscissa with a bullet at the end (in Figs 5 and 6) represents the Appell disc $r = 0$ with singular rim at $\theta = 90^\circ$ – see the Appendix for the structure of Appell space–time. A bullet is also used for the Bach–Weyl ring (at $r = 6M$ and $\rho = 9M$, respectively), and a very thick solid half-line for the Lemos–Letelier annular disc with non-singular inner edge (at $r = 6M$ and $\rho = 8M$). The Schwarzschild coordinate mesh (in plots with a black hole) and oblate spheroidal mesh (in those with an Appell ring) are dotted. The values written along the axes are in the units of M.

Note that we do not use as radial coordinate the 'circumferential' radius $R = \sqrt{g_{\phi\phi}} = \rho\,\mathrm{e}^{-\nu(\rho,z)}$ (in terms of which the physical circumference of the circle $\rho =$ constant, $z =$ constant is given by $2\pi R$). The circumferential radius is 'more physical' than ρ and generally more suitable for comparing different space–times, but only if it is unique, which is equivalent to the condition $R_{,\rho} > 0$, i.e. $\rho\nu_{,\rho} < 1$. The requirement is usually fulfilled for discs (see e.g. Bičák et al. 1993b), but not for sources for which ν

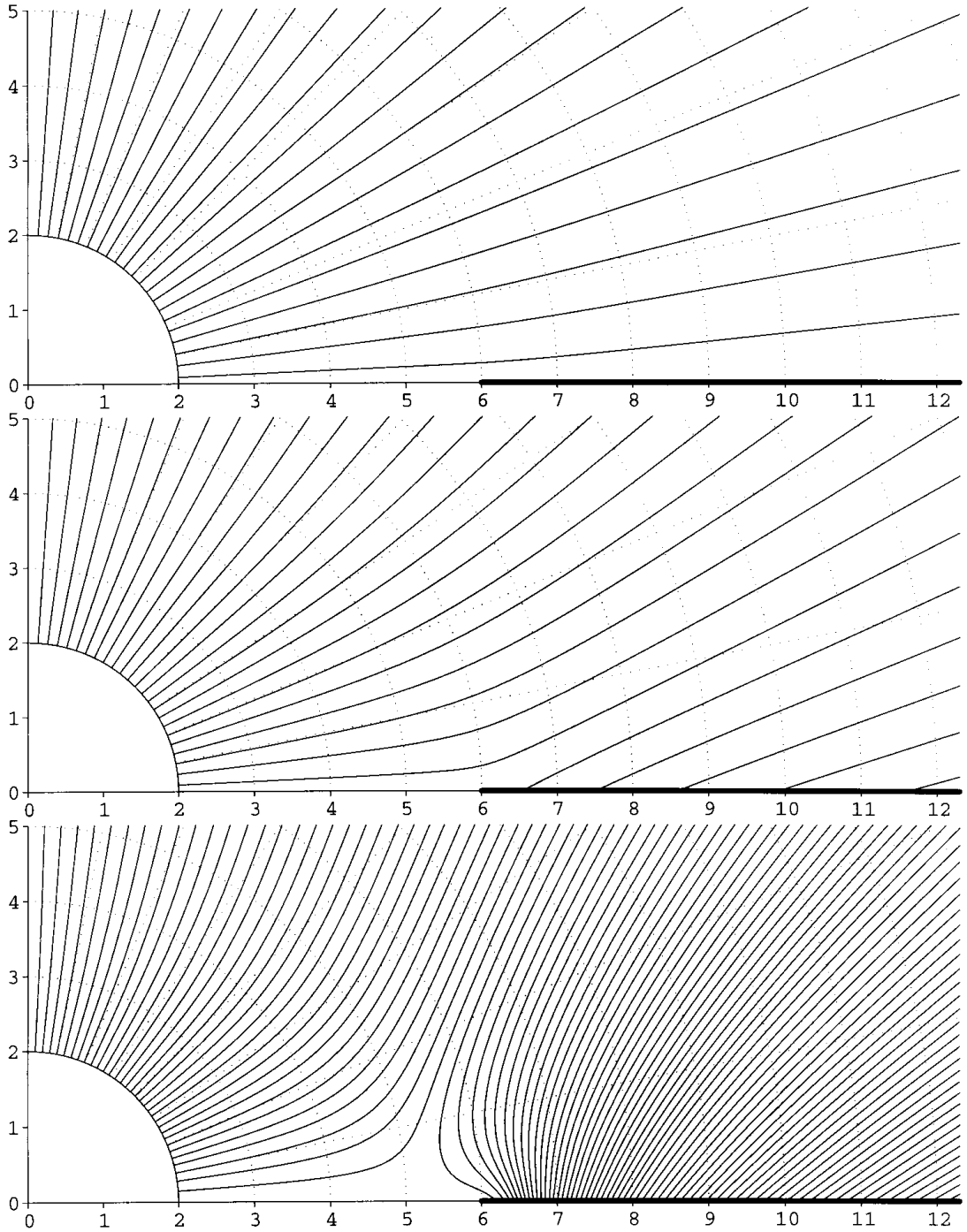

Figure 4. Field lines in the space–times of a Schwarzschild black hole (of mass M) with an equatorial Lemos–Letelier annular disc, drawn in Schwarzschild coordinates. The disc has an inner rim at $r = 6M$ and mass $\mathcal{M} = 0.1M$, M and $10M$ as taken from top to bottom.

is singular somewhere. This, however, is typical for rings – for the Bach–Weyl solution (34), for example, $k = 1$ and $\nu = -\mathcal{M}K(1)/(\pi b) = -\infty$ at the ring itself. Fig. 7 illustrates the dependence $R = R(\rho)$ in the equatorial plane of space–times of the Bach–Weyl ring and the Lemos–Letelier annular disc. Note that Chakrabarti (1988) considered the Bach–Weyl ring (around Schwarzschild hole) at $\rho = b$, or $r = r_c$, and thus at infinite circumferential radius $\rho\,\mathrm{e}^{-\nu} = r\,\mathrm{e}^{-\nu_{\mathrm{ring}}}$ ($\theta = 90°$), so his figs 2 and 3 are plotted against ρ and r (respectively) rather than against circumferential radius ($\omega \equiv r\,\mathrm{e}^{-\psi_t}$ in the original notation) as claimed – the ring could not be at $\omega_c = 8M$; cf. fig. 1 of Khanna & Chakrabarti (1992).

Figs 3–6 show that the additional sources have an expectable effect on the 'background' field: the field lines bend towards the external ring or disc, and the greater is its mass, the more of them end there. The singular ring clearly generates stronger field than the extended disc of the same mass. The strongest sources, however, are the central ones – they even dominate in cases when the additional matter has greater mass. Note that not only changes of the shape of the

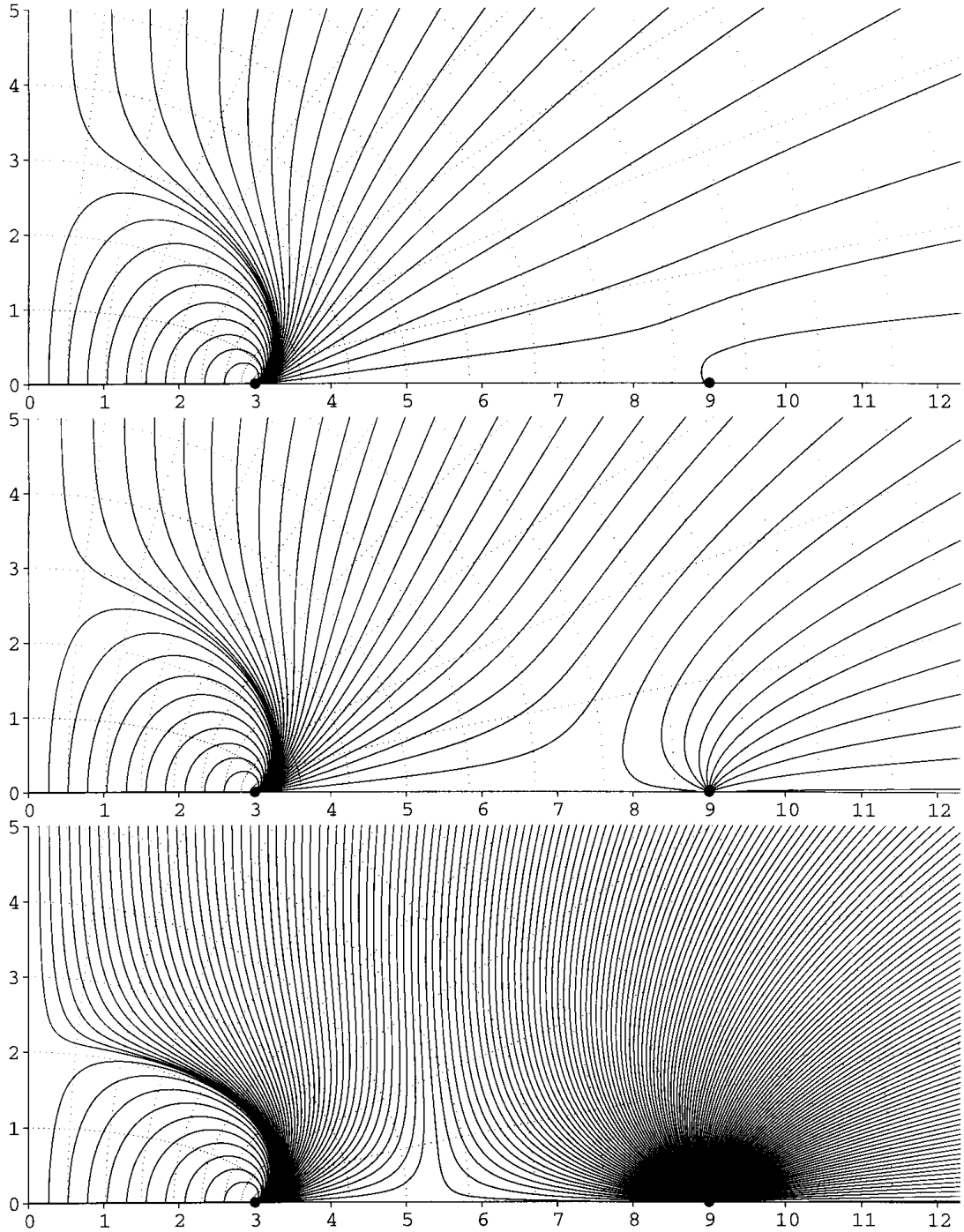

Figure 5. Field lines in the space–times of the Appell ring (of mass M and radius $a = 3M$) with a Bach–Weyl ring, drawn in Weyl coordinates. The Bach–Weyl ring is placed at $\theta = 90°$, $\rho = 9M$ and has mass $\mathcal{M} = 0.1M$, M and $10M$ as taken from top to bottom.

field are illustrated, but also its intensity is roughly indicated by density of the field lines.

5 DISTORTION OF THE SCHWARZSCHILD HORIZON BECAUSE OF AN EXTERNAL SOURCE

Geroch & Hartle (1982) analysed thoroughly the properties of static axisymmetric (Weyl) black holes distorted by an external matter distribution. They showed that the horizon of any Weyl black hole must have either spherical or toroidal topology; if the external matter has a positive energy density, then only spherical topology is possible (Hawking 1972). Below we depict the deformation of the Schwarzschild horizon induced by the presence of an external equatorial ring or disc.

In the static case, the black hole horizon is the set of points at which the static Killing field $\partial/\partial t$ becomes null, while the norm of the axisymmetric Killing field $\partial/\partial\phi$ remains bounded, i.e. where $g_{tt} = -\mathrm{e}^{2\nu} = 0$ and $g_{\phi\phi} = \mathrm{e}^{-2\nu}\rho^2 < \infty$. This implies $\rho = 0$, thus

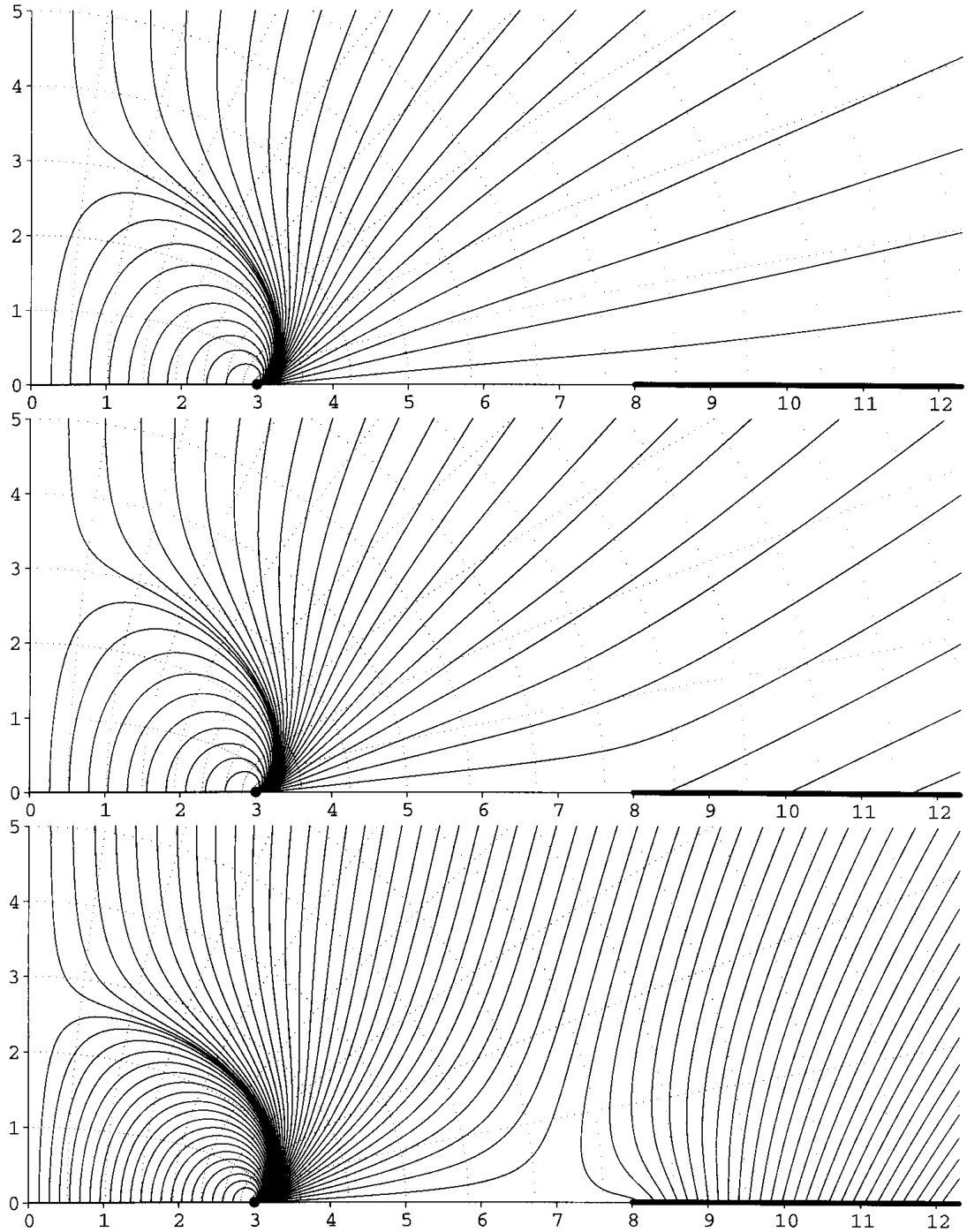

Figure 6. Field lines in the space–times of the Appell ring (of mass M and radius $a = 3M$) with an equatorial Lemos–Letelier annular disc, drawn in Weyl coordinates. The disc has an inner rim at $\rho = 8M$ and mass $\mathcal{M} = 0.1M$, M and $10M$ as taken from top to bottom.

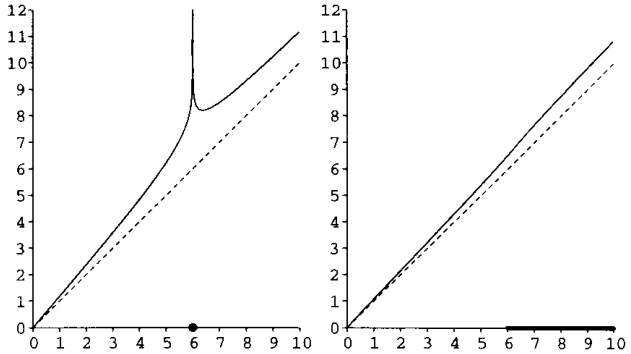

Figure 7. Circumferential radius R as a function of ρ in the equatorial plane ($z = 0$) of the Bach–Weyl ring with radius $b = 6\mathcal{M}$ (left plot) and in that of the Lemos–Letelier annular disc with inner rim at $b = 6\mathcal{M}$ (right plot). The condition of uniqueness, $R_{,\rho} > 0$, is clearly not satisfied for the ring, whereas it is for the disc. (Note that for a disc surrounding a Schwarzschild hole at the Schwarzschild radius $r = 6M$, this would only become untrue in an extremely massive case, $\mathcal{M} > 12.6M$.) The line $R = \rho$ is indicated for comparison.

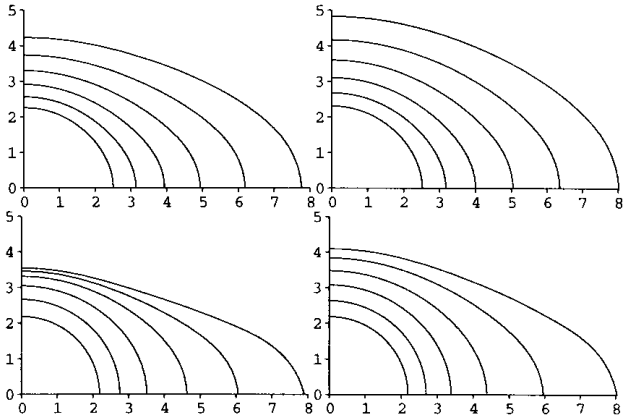

Figure 8. Distortion of the Schwarzschild horizon caused by the external Bach–Weyl ring (left plots) and by the external Lemos–Letelier annular disc (right plots). The intrinsic shape of the horizon, given by the function $R_{\rm H}(\theta)$, changes with the mass (top plots) and Schwarzschild radius (bottom plots) of the additional sources. As expected, the horizon inflates towards the external source when decreasing the radius or increasing the mass of the latter. However, quite unrealistic values must be chosen in order to raise an evident flattening: in the top plots, $r/M = 2.2$ with $\mathcal{M}/M = 0.15$, 0.3, 0.45, …, 0.9 for the ring, and $r/M = 2.1$ with $\mathcal{M}/M = 0.25$, 0.5, 0.75, …, 1.5 for the disc; in the bottom plots, $\mathcal{M}/M = 0.63$ with $r/M = 8$, 3.2, 2.5, 2.25, 2.15, 2.1 for the ring, and $\mathcal{M}/M = 1.05$ with $r/M = 6$, 2.8, 2.31, 2.15, 2.08, 2.05 for the disc.

in Weyl coordinates the horizon may appear only as a part of the symmetry axis. In Schwarzschild coordinates (also 'distorted' because of the external matter), introduced by the transformation $\rho = \sqrt{r(r-2M)}\sin\theta$, $z = (r-M)\cos\theta$, the metric appears as

$$\mathrm{d}s^2 = -(1-2M/r)\,\mathrm{e}^{2\nu_{\rm ext}}\,\mathrm{d}t^2 + \frac{\mathrm{e}^{2(\lambda_{\rm ext}-\nu_{\rm ext})}}{1-2M/r}\,\mathrm{d}r^2 + r^2\,\mathrm{e}^{-2\nu_{\rm ext}}(\mathrm{e}^{2\lambda_{\rm ext}}\,\mathrm{d}\theta^2 + \sin^2\theta\,\mathrm{d}\phi^2) \tag{60}$$

by using (12), (14) and (18) with $l = M$; we denote $\lambda_{\rm ext} = \lambda - \lambda_{\rm Schw}$, where

$$\lambda_{\rm Schw} = \frac{1}{2}\ln\frac{r^2-2Mr}{r^2-2Mr+M^2\sin^2\theta}.$$

On the horizon, $\rho = 0$ implies $\lambda = 0$ and $r = 2M$, so the metric reduces to

$$\mathrm{d}s^2 = R_{\rm H}^2(\mathrm{d}\theta^2 + \sin^2\theta\,\mathrm{d}\phi^2), \tag{61}$$

where $R_{\rm H} = \sqrt{g_{\theta\theta}(r=2M,\theta)} = 2M\,\mathrm{e}^{-\nu_{\rm ext}(r=2M,\theta)}$ is the (latitudinal) circumferential radius of the horizon (then $2\int_0^\pi R_{\rm H}(\theta)\,\mathrm{d}\theta$ is the proper poloidal circumference of the horizon and $2\pi R_{\rm H}\sin\theta$ its proper azimuthal circumference at given θ). The dependence of the function $R_{\rm H} = R_{\rm H}(\theta)$ (which gives the proper shape of the horizon) on parameters (mass or/and position) of the external source reveals the response of the horizon to the presence of this source.

For the equatorial Bach–Weyl ring (with mass $\mathcal{M}$ and radius $\rho = b$) we have, from (34),

$$\nu_{\rm ext}(r=2M) = -\frac{\mathcal{M}}{\sqrt{b^2+M^2\cos^2\theta}}, \tag{62}$$

because, on the horizon, $k = 0$, $K(0) = \pi/2$ and $d_2 = \sqrt{b^2+z^2} = \sqrt{b^2+M^2\cos^2\theta}$ in Schwarzschild coordinates (the prolate ones used in Section 3.1, with $l = M$). Thus the horizon is of oblate shape (it inflates towards the superposed ring; cf. Chakrabarti 1988), its radius

$$R_{\rm H} = 2M\exp\left(\frac{\mathcal{M}}{\sqrt{b^2+M^2\cos^2\theta}}\right) \tag{63}$$

decreasing monotonically when going from the equatorial plane to the axis.

To find the shape of a Schwarzschild black hole surrounded by an equatorial Lemos–Letelier annular disc (with mass $\mathcal{M}$ and inner edge at $\rho = b$), one must transform the expression (45) from the oblate coordinates of Sections 3.2 and 3.4 to Schwarzschild coordinates and evaluate it at the horizon. This yields $r^2 + b^2\sin^2\theta \to M^2\cos^2\theta$, $2r^2 \mp b^2\sin^2\theta \to 2M^2\cos^2\theta$ and $b|\cos\theta| \to b$, so

$$\nu_{\rm ext}\,(r=2M) = -\frac{2\mathcal{M}}{\pi M^3|\cos\theta|^3} \times\left[(b^2+M^2\cos^2\theta)\mathrm{arccot}\left(\frac{b}{M|\cos\theta|}\right) - Mb|\cos\theta|\right]. \tag{64}$$

Inflating towards the external source, the horizon is again oblate. Fig. 8 shows its shape for several different masses and radii of the Bach–Weyl ring and Lemos–Letelier annular disc. Note that Wild, Kerns & Drish (1981) found that the external magnetic field directed along the symmetry axis has the opposite effect (on a Kerr black hole): it stretches the horizon along the axis.

It is interesting to check whether the Gaussian curvature of the horizon, which is constant and positive ($\mathcal{R}_{\rm H} = 1/4M^2$) for a Schwarzschild black hole, can somewhere become negative because of the presence of the external sources. From its definition (e.g. Thorne et al. 1986, equation (6.15a)),

$$\mathcal{R}_{\rm H} = -\frac{1}{R_{\rm H}^2\sin\theta}\left[\frac{(R_{\rm H}\sin\theta)_{,\theta}}{R_{\rm H}}\right]_{,\theta}, \tag{65}$$

we obtain

$$\mathcal{R}_{\rm H} = R_{\rm H}^{-2}(1 + \nu_{{\rm ext},\theta}\cot\theta + \nu_{{\rm ext},\theta\theta}). \tag{66}$$

Hence, for a Bach–Weyl ring, $\mathcal{R}_{\rm H}$ is always positive in the

equatorial plane,

$$\mathcal{R}_{\rm H} = \frac{1}{4M^2\exp(2\mathcal{M}/b)}\left(1+\frac{\mathcal{M}M^2}{b^3}\right), \tag{67}$$

whereas on the axis one has

$$\mathcal{R}_{\rm H} = \frac{1}{4M^2\exp(2\mathcal{M}/\sqrt{b^2+M^2})}\left(1-\frac{2\mathcal{M}M^2}{(b^2+M^2)^{3/2}}\right), \tag{68}$$

which *can* turn negative, though only for large values of $\mathcal{M}$ (even for a ring just above the horizon, $b \ll M$, it would require $\mathcal{M} \doteq M/2$).

Note that Will (1974) came to a similar conclusion (for a ring) perturbatively. Demianski (1976) and Chrzanowski (1976) calculated the perturbation of a *Kerr* black hole by an equatorial ring using the Newman–Penrose formalism; here the rotation of the hole itself flattens the horizon – the latter has negative $\mathcal{R}_{\rm H}(\theta = 0)$ for the values of specific angular momentum a bigger than $\sqrt{3}M/2$ (Smarr 1973). A similar approach was employed by Hartle (1973 and 1974) to analyse the shape of the weak tide raised on a non-rotating and slowly rotating black hole by an exterior source. The horizon distortion has also appeared in numerical stationary space–times generated by (rotating) black holes and equatorial discs. Lanza (1992) considered thin discs and – interestingly – found the resulting holes *prolate* in some cases; in contrast, Nishida & Eriguchi (1994) always ended up with oblate shapes for thick toroids.

ACKNOWLEDGMENTS

OS thanks Professor Marek Abramowicz for hospitality and support at the Department of Astronomy and Astrophysics of the Göteborg University and Chalmers Technical University, where our interest in the subject originated some years ago. We thank Professor Jiří Bičák for stimulating discussions and acknowledge support from the grants GACR-202/99/0261 of the Grant Agency of the Czech Republic and GAUK-230/96 of the Charles University.

REFERENCES

Abramowicz M. A., 1987, in MacCallum M. A. H., ed., GR-11, Proc. 11th Int. Conf. on Gen. Rel. Grav. Cambridge Univ. Press, Cambridge, p. 1
Abramowicz M. A., Curir A., Schwarzenberg-Czerny A., Wilson R. E., 1984, MNRAS, 208, 279
Abramowicz M. A., Nurowski P., Wex N., 1993, Class. Quantum Grav., 10, L183
Alekseev G. A., Garcia A. A., 1996, Phys. Rev. D, 53, 1853
Aliev A. N., Gal'tsov D. V., 1989, Sov. Phys. – Usp., 32, 75
Bach R., Weyl H., 1922, Math. Zeit., 13, 134 (in German)
Bardeen J. M., 1970, Nat, 226, 64
Bardeen J. M., Petterson J. A., 1975, ApJ, 195, L65
Barrabès C., Boisseau B., Israel W., 1995, MNRAS, 276, 432
Bičák J., Hoenselaers C., 1985, Phys. Rev. D, 31, 2476
Bičák J., Lynden-Bell D., Katz J., 1993a, Phys. Rev. D, 47, 4334
Bičák J., Lynden-Bell D., Pichon C., 1993b, MNRAS, 265, 126
Blandford R. D., 1987, in Hawking S. W., Israel W., eds, 300 Years of Gravitation. Cambridge Univ. Press, Cambridge, p. 277
Boyer R. H., Lindquist R. W., 1967, J. Math. Phys., 8, 265
Bretón N., Manko V. S., 1995, Class. Quantum Grav., 12, 1969
Carter B., 1968, Phys. Rev., 174, 1559
Chakrabarti S. K., 1988, JA&A, 9, 49
Chandrasekhar S., 1979, in Hawking S. W., Israel W., eds, General Relativity – An Einstein Centenary Survey. Cambridge Univ. Press, Cambridge, p. 370
Chaudhuri S., Das K. C., 1997a, Gen. Rel. Grav., 29, 75
Chaudhuri S., Das K. C., 1997b, J. Math. Phys., 38, 5792
Chrzanowski P. L., 1975, Phys. Rev. D, 11, 2042
Chrzanowski P. L., 1976, Phys. Rev. D, 13, 806
Cosgrove C. M., 1980, J. Math. Phys., 21, 2417
Cosgrove C. M., 1981, J. Math. Phys., 22, 2624
Cosgrove C. M., 1982, J. Math. Phys., 23, 615
Demianski M., 1976, Gen. Rel. Grav., 7, 551
Dietz W., Hoenselaers C., 1985, Ann. Phys. (NY), 165, 319
Fernandes J. F. Q., Lun A. W. C., 1996, J. Math. Phys., 37, 836
Fernandes J. F. Q., Lun A. W. C., 1997, J. Math. Phys., 38, 330
Geroch R., Hartle J. B., 1982, J. Math. Phys., 23, 680
Gibbons G., 1980, Proc. R. Soc. London, Ser. A, 372, 535
Gleiser R. J., Pullin J. A., 1989, Class. Quantum Grav., 6, 977
Goodman J., Narayan R., 1988, MNRAS, 231, 17
Greene R. D., Schucking E. L., Vishveshwara C. V., 1975, J. Math. Phys., 16, 153
Hamity V. H., 1976, Phys. Lett. A, 56, 77
Hartle J. B., 1973, Phys. Rev. D, 8, 1010
Hartle J. B., 1974, Phys. Rev. D, 9, 2749
Hawking S. W., 1972, Commun. Math. Phys., 25, 152
Hoenselaers C., 1990, Class. Quantum Grav., 7, 581
Hoenselaers C., 1993, in Chinea F. J., Gonzáles-Romero L. M., eds, Lecture Notes in Physics 423, Rotating Objects and Relativistic Physics. Springer-Verlag, Berlin, Heidelberg, p. 29
Hoenselaers C., 1995, Class. Quantum Grav., 12, 141
Hoenselaers C., Dietz W., eds, 1984, Lecture Notes in Physics 205, Solutions of Einstein's Equations: Techniques and Results. Springer-Verlag, Berlin, Heidelberg
Israel W., 1970, Phys. Rev. D, 2, 641
Jantzen R. T., Carini P., Bini D., 1992, Ann. Phys. (NY), 215, 1
Kato S., Fukue J., Mineshige S., 1998, Black-Hole Accretion Disks. Kyoto Univ. Press, Kyoto
Keres H., 1967, Zh. Eksp. Teor. Fiz., 25, 504
Khanna R., Chakrabarti S. K., 1992, MNRAS, 259, 1
Lanza A., 1992, ApJ, 389, 141
Lemos J. P. S., Letelier P. S., 1994, Phys. Rev. D, 49, 5135
Letelier P. S., Oliveira S. R., 1987, J. Math. Phys., 28, 165
Letelier P. S., Oliveira S. R., 1998, Class. Quantum Grav., 15, 421
Letelier P. S., 1989, Class. Quantum Grav., 6, 875
Levi-Civita T., 1919, Atti Accad. Lincei Rend., 28, 3 (in Italian)
Linet B., 1977, Phys. Lett. A, 60, 395
López C. A., 1981, Nuovo Cimento B, 66, 17
McManus D., 1991, Class. Quantum Grav., 8, 863
Manko V. S., Novikov I. D., 1992, Class. Quantum Grav., 9, 2477
Manko V. S., Martún J., Ruiz E., 1994, J. Math. Phys., 35, 6644
Misner C. W., Thorne K. S., Wheeler J. A., 1973, Gravitation. Freeman, San Francisco
Morgan T., Morgan L., 1969, Phys. Rev., 183, 1097 (erratum 188, 2544)
Nishida S., Eriguchi Y., 1994, ApJ, 427, 429
Nishida S., Eriguchi Y., 1996, ApJ, 461, 320
Paczyński B., Wiita P. J., 1980, A&A, 88, 23
Parker L., Ruffini R., Wilkins D., 1973, Phys. Rev. D, 7, 2874
Pfister H., Schedel Ch., 1987, Class. Quantum Grav., 4, 141
Punsly B., 1990, Gen. Rel. Grav., 22, 1169
Quevedo H., 1992, Phys. Rev. D, 45, 1174
Quevedo H., Mashhoon B., 1991, Phys. Rev. D, 43, 3902
Rees M. J., 1998, in Wald R. M., ed., Black Holes and Relativistic Stars. Univ. Chicago Press, Chicago, p. 79
Scott S. M., Szekeres P., 1986, Gen. Rel. Grav., 18, 557
Semerák O., 1995, Nuovo Cimento B, 110, 973
Semerák O., Žáček M., Zellerin T., 1999, MNRAS, (Paper II, this issue), in press
Shlosman I., Begelman M. C., 1987, Nat, 329, 810
Smarr L., 1973, Phys. Rev. D, 7, 289

Synge J. L., 1960, Relativity: The General Theory. North-Holland, Amsterdam, Chapt. VIII.1
Tanabe Y., 1979, J. Math. Phys., 20, 1486
Tertychniy S. I., 1990, Class. Quantum Grav., 7, 1345
Teukolsky S. A., 1973, ApJ, 185, 635
Thorne K. S., Price R. H., Macdonald D. A., eds, 1986, Black Holes: The Membrane Paradigm. Yale Univ. Press, New Haven
Vein P. R., 1985, Class. Quantum Grav., 2, 899
Weyl H., 1917, Ann. Phys. (Leipzig), 54, 117 (in German)
Wild W. J., Kerns R. M., Drish W. F. Jr, 1981, Phys. Rev. D, 23, 829
Will C. M., 1974, ApJ, 191, 521
Zipoy D. M., 1966, J. Math. Phys., 7, 1137

APPENDIX A: KERR AND APPELL SOLUTIONS: SIMILARITIES AND DIFFERENCES

The Kerr metric is astrophysically the most important axisymmetric solution of the Einstein equations. In Boyer–Lindquist oblate spheroidal coordinates (t, r, θ, ϕ) it reads (Misner, Thorne & Wheeler 1973, p. 878)

$$\mathrm{d}s^2 = -\left(1-\frac{2Mr}{\Sigma}\right)\mathrm{d}t^2 - \frac{4Mar\sin^2\theta}{\Sigma}\mathrm{d}t\,\mathrm{d}\phi + \frac{\mathcal{A}}{\Sigma}\sin^2\theta\,\mathrm{d}\phi^2 + \frac{\Sigma}{\Delta}\mathrm{d}r^2 + \Sigma\,\mathrm{d}\theta^2, \tag{A1}$$

where M and a (>0) denote mass and specific rotational angular momentum of the source and $\Delta = r^2 - 2Mr + a^2$, $\Sigma = r^2 + a^2\cos^2\theta$, $\mathcal{A} = (r^2+a^2)^2 - \Delta a^2\sin^2\theta$. Outside the horizons ($\Delta > 0$), the metric is stationary and in fact describes the most general space–time around an isolated uncharged stationary black hole. The innermost part of the manifold (in particular the ring-like character of the singularity) is better represented in the Kerr–Schild cylindrical coordinates,

$$\rho = \sqrt{r^2+a^2}\,\sin\theta, \qquad z = a\cos\theta. \tag{A2}$$

In the words of Israel (1970):

> A key feature of the Kerr geometry is an equatorial disc, centered on the axis of symmetry, which is intrinsically flat and of radius a. The ringlike boundary of the disc comprises the geometrical singularity of the metric. In addition, the disc itself has a remarkable property: As one approaches it from either above or below, r tends to zero through positive values, but (grad r) (directed outward from the disc) does not vanish. Since r has an intrinsic meaning, this must be interpreted in one of the following ways: (i) The complete Kerr manifold is defined so that $r \geqslant 0$ everywhere, and there is a discontinuity in the normal derivative of the metric across the flat disc. (ii) Alternatively, the metric remains smooth everywhere away from the ring singularity, but an observer crossing the disc $r = 0$ from a region with $r > 0$ emerges into a new asymptotically flat space characterized by $r < 0$; the two 'Riemann sheets' with $r > 0$ and $r < 0$ are to be considered as joined together on the disc $r = 0$ which serves as a branch cut.

Adopting interpretation (i), one eliminates the non-causal features that may occur at $r < 0$ ($z < 0$), in a toroidal region where $\mathcal{A} < 0$. (In this region spanned by the ring singularity, $g_{\phi\phi} < 0$, the vector $\partial/\partial\phi$ becomes time-like and thus closed time-like curves are possible. Carter 1968.) The lack of smoothness at $r = 0$ ($z = 0$, $\rho = a\sin\theta$) is ascribed to a layer of mass spread over the disc. It is made of unphysical material, rotating with supraluminal velocity and having negative effective surface mass density

$$\sigma = -\frac{M}{2\pi a^2\cos^3\theta} = -\frac{Ma}{2\pi(a^2-\rho^2)^{3/2}}. \tag{A3}$$

The density diverges to $-\infty$ as $\theta \to 90°$ ($\rho \to a$); at the singular rim it jumps to $+\infty$ and yields the finite positive net value of M. Consequently, the spherical region $r < a|\cos\theta|$ ($\rho^2 + z^2 < a^2$) is 'repulsive' in a sense that momentarily static particles ($\mathrm{d}x^i/\mathrm{d}\tau = 0$) are radially accelerated away from the disc ($\mathrm{d}^2r/\mathrm{d}\tau^2 > 0$). [Note that this conclusion was already reached by Keres (1967); see also the related papers by Hamity (1976); López (1981); McManus (1991).]

Adopting interpretation (ii), one considers the whole maximal extension of the Kerr metric by Boyer & Lindquist (1967). In the metric, the sign of r is relevant only in terms containing Mr, so the $r < 0$ sheet of the manifold can be understood to be physically the same as the $r > 0$ sheet, but with negative mass, $-M$ (thus also with negative angular momentum, $-Ma$). In other words, in

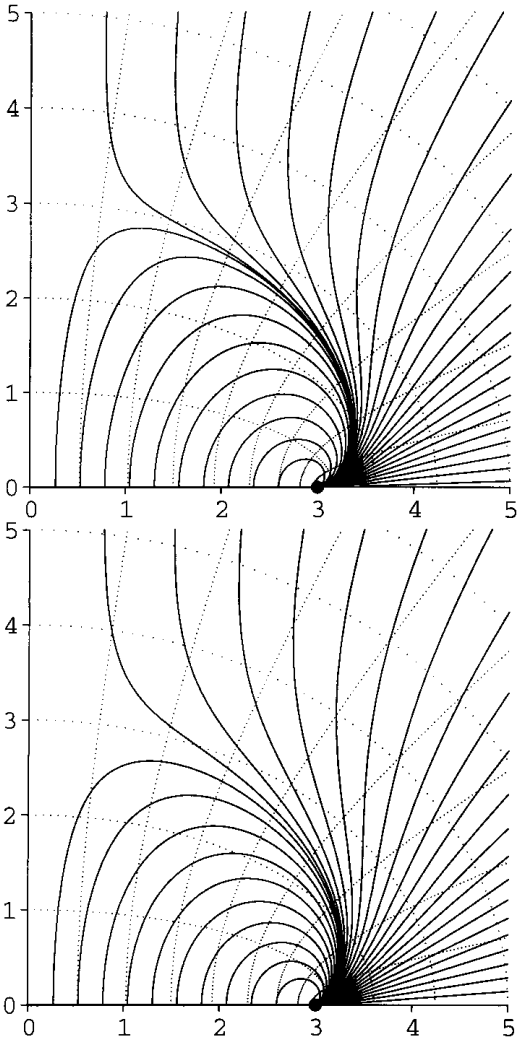

Figure A1. Gravitational field lines (defined according to Section 4) of the Kerr space–time, depicted in Kerr–Schild coordinates (top plot), and of the Appell space–time, depicted in Weyl coordinates (bottom plot). The parameters of both space–times are M and $a = 3M$ and the meaning of the plots is the same as that of the plots grouped in Figs 3–6. The very close similarity of the fields is clearly visible.

the $r < 0$ sheet the gravitational field is exactly opposite to that at $r > 0$; in particular, it is 'repulsive' everywhere except for the region $(0 >) r > -a|\cos\theta|$, the dragging effects also having opposite sign. On circling twice round (through) the singular ring, one passes from $r < 0$ to $r > 0$ and back. From the $r > 0$ region, it is possible to reach the singularity only along trajectories bound to the equatorial plane (and having small angular momentum).

Almost everything summarized above is also true for the Appell solution,[4] described in Section 3.2, however, with ρ and z now being Weyl coordinates; r and θ are again related to these by equations (A2) (namely by equation 26). In the oblate coordinates, the Appell metric reads

$$\mathrm{d}s^2 = -\mathrm{e}^{-2Mr/\Sigma}\,\mathrm{d}t^2 + \mathrm{e}^{2Mr/\Sigma}(r^2 + a^2)\sin^2\theta\,\mathrm{d}\phi^2 + \mathrm{e}^{2(\lambda-\nu)}\left(\frac{\Sigma}{r^2 + a^2}\,\mathrm{d}r^2 + \Sigma\,\mathrm{d}\theta^2\right). \tag{A4}$$

Comparing this with (A1), we find that the local properties of the Kerr and Appell space–times are similar at large r, and also at small r close to the axis: in these regions, $(\lambda - \nu)$ and Mr/Σ (and thus also the Kerr dragging component $g_{t\phi} = -2Mar\sin^2\theta/\Sigma$) are small and $\Delta \simeq r^2 + a^2$. The greatest differences appear, as expected, where the Kerr space–time has a horizon ($\Delta = 0$). However, the horizon does not exist for $a > M$, and indeed the fields are also similar for very large a.

The similarity of the Kerr and the Appell fields is illustrated in Fig. A1 where the field lines of both are drawn with the same parameter a ($= 3M$) as was chosen for the Appell background considered in Section 4.

This paper has been typeset from a TEX/LATEX file prepared by the author.

[4]The described double-sheeted (or even multisheeted) topology is in fact *typical* for the Weyl solutions obtained in oblate coordinates (Zipoy 1966). At the Appell space–time, it even survives for $a \to 0$, i.e. in the Curzon limit (Scott & Szekeres 1986).